Quarterly Report – Public Page

Date of Report: 3rd Quarterly Report-June 30, 2023
Contract Number: *693JK322RA0001*
Prepared for: *DOT/PHMSA*
Project Title: Determining the Required Modifications to Safely Repurpose Existing Pipelines to Transport Pure Hydrogen and Hydrogen-Blends
Prepared by: Engineering Mechanics Corporation of Columbus
Contact Information: Gery Wilkowski, (gwilkows@emc-sq.com)
For quarterly period ending: *June 30, 2023*

1: Items Completed During this Quarterly Period:

The following items were delivered in this quarterly period. We have caught up on all items that were not completed last quarter.

Item #	Task #	Activity/Deliverable	Title	Federal Cost	Cost Share
4	1	Literature Review	Perform Literature Review	$14,000	$0
5	2	Identify potential limitations in components and pipeline conditions	Potential component and condition limitations identified	$8,000	$0
6	5	Assess critical flaw sizes and respective detection thresholds	Critical flaw sizes and thresholds assessed	$25,000	$20,000
9	2	Identify potential limitations in components and pipeline conditions	Potential component and condition limitations identified	$8,000	$0
12	5	Assess critical flaw sizes and respective detection thresholds	Critical flaw sizes and thresholds assessed	$25,000	$20,000
13	8	3rd Quarterly Status Report	Submit 3rd quarterly report	$2,500	$0

2: Items Not Completed During this Quarterly Period:

Item #	Task #	Activity/Deliverable	Title	Federal Cost	Cost Share
8	1	Literature Review	Perform Literature Review	$14,000	$0
10	3	Task 3 – Evaluate metallic and non-metallic components for retrofit or replacement	Components retrofit or replacement evaluated	$20,000	$0

3: Project Financial Tracking During this Quarterly Period:

Note, the financial tracking chart in the prior quarterly report was off one quarter since it used the proposal assumption of starting in the 3rd Quarter of 2022. The project started in October of 2022. This has been corrected in the chart below.

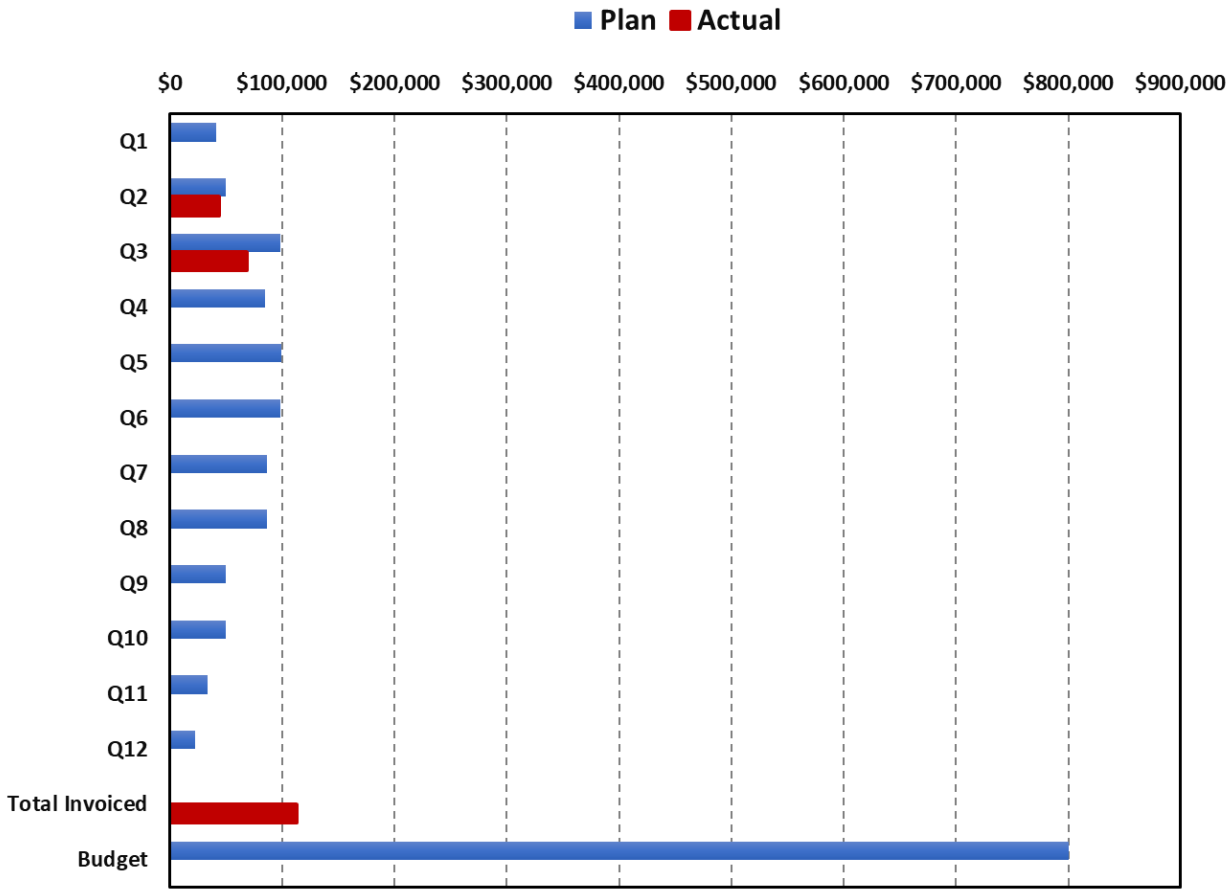

4: Project Technical Status –

Work has progressed at a significantly increased pace. Below are the summaries of these efforts.

Task 1 – Literature Review

The literature review report for this project on repurposing pipelines for hydrogen service is in the final writing process but will take one more month to complete. A companion literature review was completed in a complementary DOT/PHMSA project on *Reviewing of Integrity Threat Characterization Resulting from Hydrogen Gas Pipeline Service - 693JK32210013POTA.* That review report focuses on differences of material behavior in the presence of hydrogen, and in particular mechanical properties that may affect the structural integrity of new or repurposed hydrogen pipelines. That separate literature review should be of help to this project TTI since it covers other topics and the literature report for this project. We will send him a complimentary copy.

Task 2 – Identify Potential Limitations in Components and Pipeline Conditions

Steel Surface Condition

The exposure of steel pipelines to molecular hydrogen for blended or pure hydrogen service is a topic of considerable concern, and frankly much speculation currently. The steel properties are degraded only if there is atomic hydrogen, so the molecular hydrogen inside the pipeline needs to reduce itself to two atomic hydrogen atoms in the steel. This doesn't occur readily.

If the steel is bare metal with no oxide film, then the molecular hydrogen, especially at higher stressed locations will want to diffuse slowly into the steel surface. The atomic hydrogen will then transport towards the higher stressed regions, and cause changes in the mechanical performance properties. In autoclave testing, such as at Sandia and other places (Emc^2 also has some autoclaved for hydrogen testing), the test specimens are machined and ground to a smooth finish. They have some exposure to humidity in the air prior to being put in the autoclave, but there is no observable oxide on the surface. The entire specimen is then exposed to hydrogen on all sides. Conducting some fatigue crack growth in the autoclave with the hydrogen also creates additional fresh surfaces for the molecular hydrogen to disassociate into atomic hydrogen into the steel sample. On the other hand, a pipeline that might be repurposed for hydrogen surface will have corrosion and other products build up on the surface under years of service. Some investigators believe those internal pragmatic surface conditions will stop or greatly retard any hydrogen from getting in the steel. So, it might be interesting to have some hydrogen permeation studies conducted on steel samples with the hydrogen on the natural ID surface of a pipeline. But the sample should also be loaded in tension to a stress level, like 72% SMYS. These may have to be long-term exposure tests and have reference bare metal samples as well. Hence, one of the key aspects is the inside surface conditions that can act as a barrier. That aspect comes into play even if there were to be full-scale pipe tests, i.e., how long should the pipe be held at pressure with hydrogen and what should the ID surface preparation be.

Fatigue Life Aspects

Much discussion has been raised about the effects of hydrogen on the fatigue crack growth rates. The rates are accelerated at high cyclic stress intensity factors (ΔK), which means that the applied stresses (i.e., pressure) need to have a high-pressure fluctuation. Normally natural gas transportation lines have very small pressure fluctuation, ~5% perhaps two times a day. This gives a low ΔK, so that the crack growth rate is not accelerated there until perhaps near the end of life. The lower ΔK values in air and hydrogen are shown in Figure 1.

Grey hydrogen pipelines transporting hydrogen created from steam methane reforming (SMR) in refineries can produce large amounts of hydrogen at a relatively constant pressure and flow rate so that the cyclic pressure levels are small and fatigue crack growth may not be that high of a concern.

Green hydrogen lines that create hydrogen from solar cells and electrolysis are inherently subject to much larger pressure cycles. This is because at night there is no solar power to keep the hydrogen flow rate, so the pipeline pressure bleeds down more significantly. Such a pipeline system should account for the larger ΔK on the fatigue crack growth, see difference of hydrogen and air fatigue crack growth rates (da/dn) when ΔK is greater than 15 MPa√m.

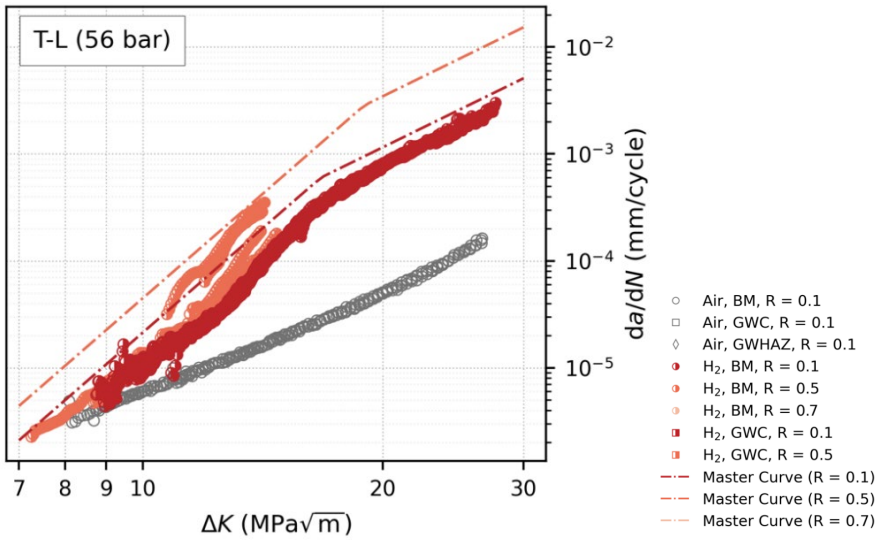

Figure 1 FCGR test data at 56 bar hydrogen

Finally on the fatigue analysis side for design of new pipelines, the traditional S-N fatigue life evaluation procedure used in traditional standards design tends to show much lower effects of hydrogen, see Figure 2*. A traditional design approach for S-N fatigue life evaluation is to use a safety factor of 2 on stress or 20 on cycles. The red curves in Figure 2 are for a SF of 2 on stress for the methane curve. This SF approach appears to cover any of the effects of hydrogen on the S-N fatigue life evaluation. A factor of 20 on cycles would also cover the hydrogen effects with less conservatism.

* Note the original figures from Report 151 include an error in the legend for X52 and X60 steels. In both these figures, the MH should have been indicated by x and MHC is indicated by □. These symbols were fixed in the top two graphs in Figure 2

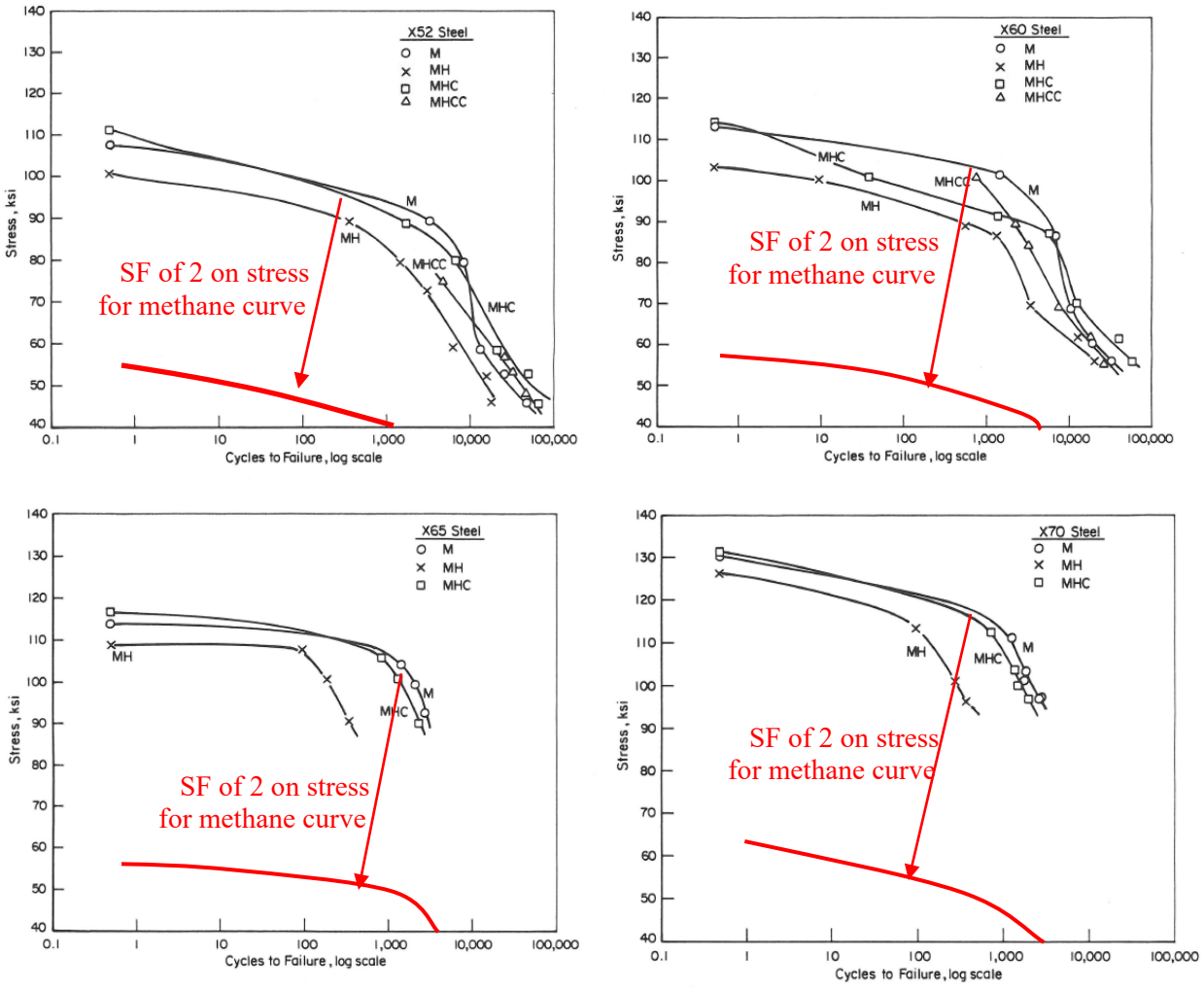

Figure 2 S-N fatigue curves for pre-1985 line-pipe steels pure methane (M); 60% hydrogen and methane (MH); methane, 60% hydrogen and 24% CO (MHC); and methane, 60% hydrogen, 25% CO and 10% CO_2 (MHCC)

Operating Temperature Considerations

The term "hydrogen embrittlement" implies to the layman that the material becomes more brittle with hydrogen. Yet most of the data developed to date show changes in percent elongation in tensile tests, increases of fatigue crack growth rates, and reductions of the upper-shelf toughness.

Most of the fracture toughness data in hydrogen autoclaves has been developed at ambient room temperature using highly constrained C(T) specimens. That is because it is tremendously more difficult to cool the whole autoclave for lower temperature testing. From much of our past work, and looking at hundreds of pipe tests, a surface-cracked pipe will have a much lower brittle-to-ductile transition temperature than a C(T) or Charpy test. For virtually all base metals of linepipe steel, there will be ductile crack initiation (start of ductile tearing) at much lower temperatures than the normal minimum ground temperature. The more important case might be for vintage LF-ERW fusion lines where the few hard ones might initiate in a brittle manner, but many more of them have surface crack transition temperatures closer to the minimum operating temperature. Hence the potential transition temperature shift that might come from "hydrogen embrittlement" could have an impact on the repurposing of those

vintage pipelines for hydrogen service. Unfortunately, there is no such data on the temperature effects for LF-ERW weld toughness.

Other Types of Pragmatic Pipeline Integrity Challenges

Other than axial cracks in the pipe body or seam welds, some additional pragmatic integrity challenges are the following.

- External SCC colonies – the question here is how the internal hydrogen might interact with the SCC crack growth. This is an aspect that the PRCI-EFI is planning to evaluate experimentally.
- Axial crack behavior with a prior hydrotest – some sensitivity studies were conducted to see the change in the hydrogen concentrations in an axial crack with and without a prior hydrotest. Interestingly, the results from our preliminary ABAQUS analysis in Figure 3 show that the hydrogen concentration may be 4 to 6 times lower after a hydrotest compared to the identical crack not experiencing the hydrotest, see Figure 11. The reason for the lowering of the hydrogen concentration after the hydrotest is that the plasticity that develops at the crack region when unloaded after the hydrotest becomes a compressive stress, and upon further loading, the hydrostatic stresses are lowered, and hence the hydrogen concentration is lower. Those trends will be confirmed with the more enhanced hydrogen transport analysis procedures from University of Akron (see Subtask 5.1) when that methodology is mature enough.

	Peak Hydrostatic Pressure (MPa)	Peak Hydrogen Concentration (ppm)
50% SMYS		
Base Case (load to 900 psig)	-997	55.5
Hydro #1 (load to 1125 psig then drop to 900 psig)	-677	11.1
Hydro #2 (load to 1350 psig then drop to 900 psig)	-502	8.1
60% SMYS		
Base Case (load to 1080 psig)	-1023	67.1
Hydro #1 (load to 1350 psig then drop to 1080 psig)	-713	13.1
Hydro #2 (load to 1620 psig then drop to 1080 psig)	-620	10.4
72% SMYS		
Base Case (load to 1296 psig)	-1066	78.7
Hydro #1 (load to 1620 psig then drop to 1296 psig)	-776	16.8
Hydro #2 (load to 1944 psig then drop to 1296 psig)	-678	16.0

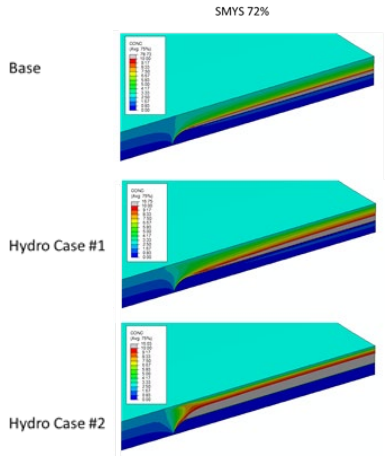

Figure 3 FE calculation showing benefits of preservice hydrotest on cracked pipe for hydrogen service

- Dents can failure by fatigue crack growth, but in addition to that there is prior plastic deformation. That plastic strain will contribute to the hydrogen density on the ID tensile strained region. Hydrogen wants to migrate to the higher stressed regions regardless of if there is a crack there or just some prior plastic deformation. This is discussed in Subtask 5.1. If there is a crack present, then there will be a further perturbation of the hydrogen concentration moving ahead of the crack. The PRCI EFI group is planning some full-scale hydrogen tests on dents.
- Wrinkle bends in vintage pipes are locations of prior plastic strains. The hydrogen will concentrate on the tensile surface because of those plastic strains and move inwards if a crack develops. This is an aspect that the PRCI-EFI is planning to evaluate experimentally.
- General corrosion can cause a slight increase in the hydrogen density from our initial ABAQUS calculations (see Figure 4 and Figure 5), but with the ongoing efforts in Subtask 5.1, that hydrogen concentration from the hydrostatic stresses and plastic strain combinations may change the distributions shown in Figure 4.

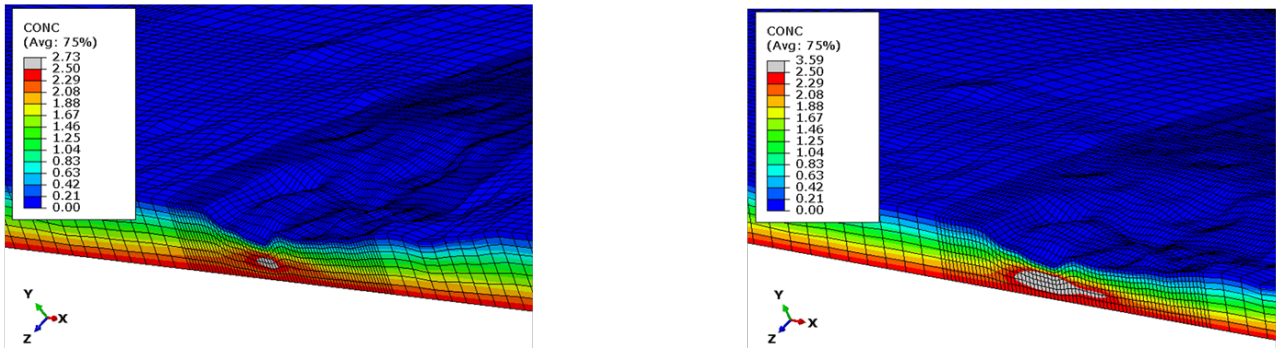

(a) Case 1 – no prior hydrotest; at 72% SMYS SMYS operation

(b) Case 2 – 1.25X hydrotest followed by 72%

Figure 4 FE model showing hydrogen density differences of corrosion patch with and without prior hydrotest

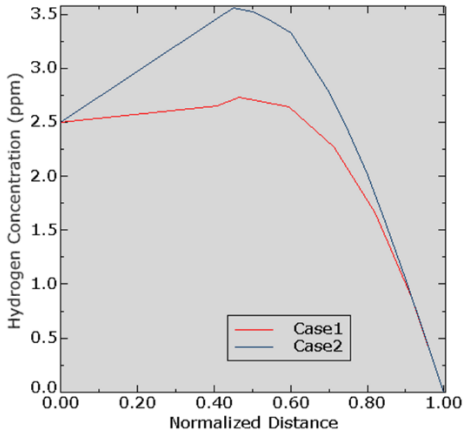

Figure 5 FE model predicted hydrogen density concentrations through the thickness at peak region

- Girth welds may also develop high hydrogen concentrations, especially at stop-start locations. In prior work Emc^2 did on refinery piping subjected to high-temperature hydrogen assisted (HTHA) cracking, we saw that the stop-start location of girth welds was the initial source of cracking. Linepipe, although not at high enough temperature to have HTHA cracking) will have higher residual stresses at the girth weld stop-start locations, as illustrated by the FE result in Figure 6. In a weld there are plastic strain of the material from thermal cooling, and high hydrostatic residual stresses.

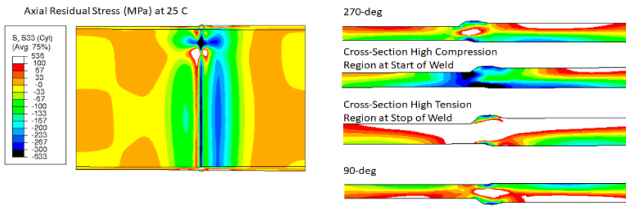

(a) Axial residual stresses at 4 locations around the circumference at 25C (stresses in MPa)

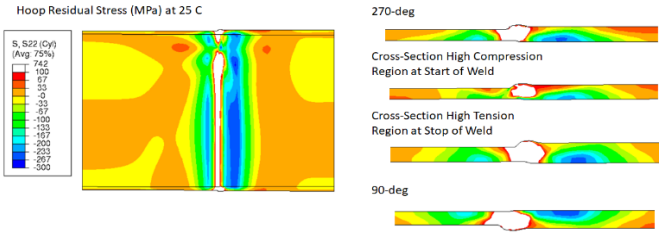

(b) Hoop residual stresses at 4 locations around the circumference at 25C (stresses in MPa)

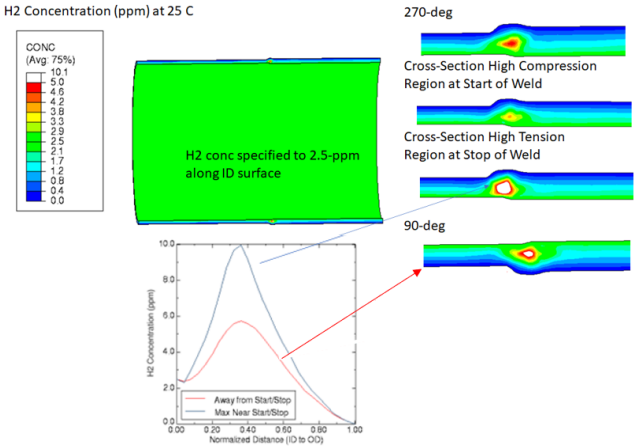

(c) Calculated H_2 concentrations at 4 locations around the circumference at 25C

Figure 6 FE simulation of weld residual stresses in a girth weld where the last-weld bead pass controlled the residual stresses, especially at the start-stop location where HTHA cracking occurred in refinery piping – and hydrogen concentration calculation using ABAQUS built in capabilities

- Hard spots are another pragmatic integrity concern in vintage pipe. This is discussed in greater detail in Section 5.2.
- Other types of welds that can be important are saddle welds for hydrogen injection nozzles, and the fillet welds in Type B repair sleeves (see Task 4 discussion).
- Gouges (usually in dents) are a particularly difficult type of flaw to evaluate. As such there is little activity associated with this type of integrity concern. This may require some future testing to determine the relative severity with and without hydrogen in bounding cases.
- Laminations are of some concern of the atomic hydrogen being trapped by the lamination and recombining to molecular hydrogen that can't move through the steel lattice. This behavior has resulted in stepwise HIC cracking and development of blisters caused by high-pressure molecular hydrogen build up by the lamination.
    - Somewhat akin to the lamination concern might be hook crack. A hook crack is formed by the outward bending of the plate material at high temperature. If there are laminations or inclusions parallel to the plate surface, then in the process of making the

ERW the is a material discontinuity there, see Figure 7. For hydrogen service, one might surmise that these hooking material discontinuities that may contain MnS inclusions, would also be trapping sites for atomic hydrogen that could subsequently recombine into molecular hydrogen, but rather than forming a blister, the bond across that region would pop open. This is a difficult integrity challenge to interrogate, perhaps other than a full-scale pipe test, or cleaver plate section testing with hydrogen only on one side of the specimen.

- This ERW hook crack hydrogen challenge and the lamination/blistering challenge involve a third hydrogen trapping mechanism (from inclusion barriers) that is not yet in any of the theoretical hydrogen transport models, see Section 5.1. This aspect should be included in the FE transport models in the future.

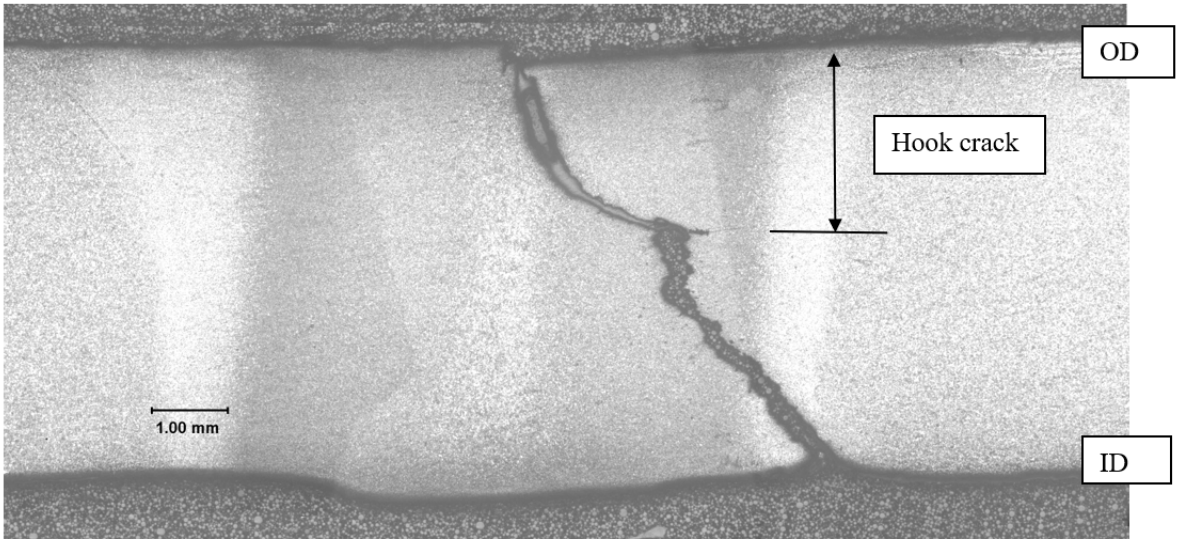

(a) Failed ERW due to a hook crack

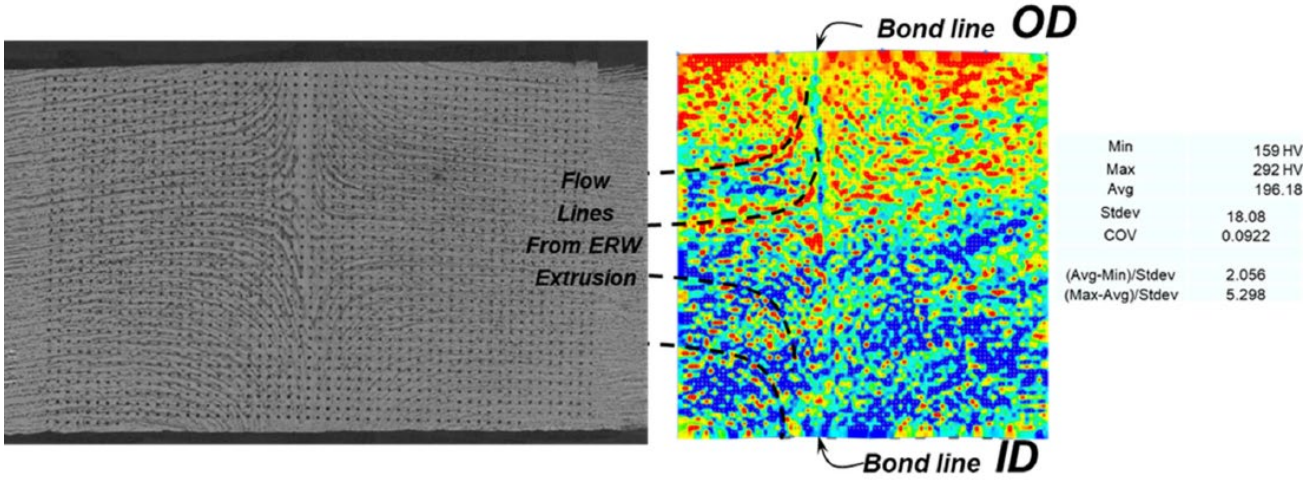

(b) Intact ERW cross-section showing flow lines with inclusion bands bending from parallel to the plate to hooking to the ID or OD surfaces – as well as hardness mapping

Figure 7 Example of a service failure from a hook crack, and inclusion bands flowing from parallel to the plate surface to hooking towards the ID or OD surface

Task 3 – Evaluate Non-metallic Components for Retrofit or Replacement

References are currently being collected to see the effects of hydrogen on composite and plastic pipes. More progress will be reported in the next quarterly report.

Task 4 – Develop Assessment and Repair Procedure for Identified Anomalies

One of the commonly used repair procedures in older pipelines is a Type B steel sleeve. A Type B repair sleeve involves taking a piece of the same size pipe, cutting it to an axial length sufficient to cover the defect of concern, and cutting the pipe segment axially to two 180-degree sections. Those two sections are fit around the pipe and welded together, preferably without side straps, see Figure 8. If there is a dent or other indentation, then a solid filler, like autobody fiber filling paste, may be used in the annular region.

The fillet welds are made in the field and perhaps are the most difficult to make without any fabrication imperfections. The fillet welds are also not stress relieved so there can be higher residual stresses. For a pipe that is in hydrogen service, or if the repair was made prior to going into hydrogen service, the fillet weld is a prime location for hydrogen damage to occur.

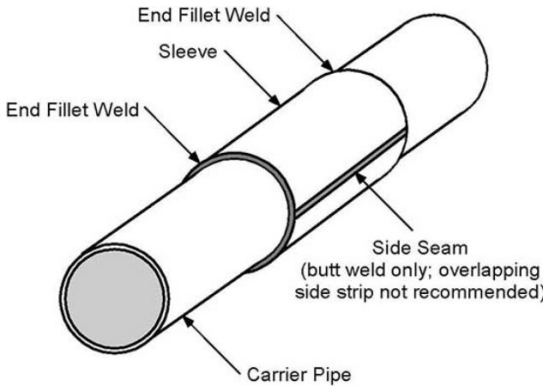

Figure 8 Illustration of a Type B repair sleeve intended to contain leakage

An initial assessment was made of the Type B fillet weld by numerical welding simulation using an axisymmetric solution. Eventually the hydrogen concentration build up will be solved for, but the key aspects are the plastic strain and the hydrostatic stresses, see discussion in Task 5.1.

In addition to examining the weld residual stresses of the fillet weld, a weld overlay procedure was used over the fillet weld regions to see if the stresses can be reduced. The weld overlay repair method has been used extensively in the nuclear piping area for repair of cracked girth weld or as a preemptive procedure to eliminate future concerns of a critical girth weld.

In Figure 9, the FE stress analysis results for the fillet weld are shown only for part of the repair sleeve and pipe area of interest. The weld overlay was applied from the center of the sleeve (the top of the pictures) down to the carrier pipe. This weld sequencing can be important as will be shown. The Type B sleeve was on a 30-inch diameter by 0.375-inch thick X52 pipe with a sleeve of the same thickness and same strength material. The internal pressure was 72% SMYS in the carrier pipe and assumed to leak into the annular area between the carrier pipe and the repair sleeve, where there was a minimal gap between the sleeve and the carrier pipe at zero pressure. On the top row is the hoop stresses, the middle row is the longitudinal stresses (although there were no applied longitudinal stresses), and the bottom row is the maximum principal stress. From left to right in each row are the; (i) initial Type B sleeve

with the fillet weld, (ii) a weld overlay equal to half the thickness of the pipe and sleeve, and (iii) a weld overlay of the full thickness of the carrier pipe.

The principal stresses in the Type B sleeve are high in the actual fillet weld. This is the area where there are more likely to be weld defects. With no defects, cracks will initiate off the toe of the fillet weld and grow into the carrier pipe, or at the root of the fillet weld and grow in either direction (through the carrier pipe or through the repair sleeve). In any of these cases there will be a high concentration of hydrogen to reduce the fatigue life and reduce the fracture toughness making the critical crack size smaller. Of the two weld overlay procedures examined, the smaller (and more economical) option seemed adequate to significantly reduce the principal stresses in the fillet weld region and even put the root of the fillet weld into compression.

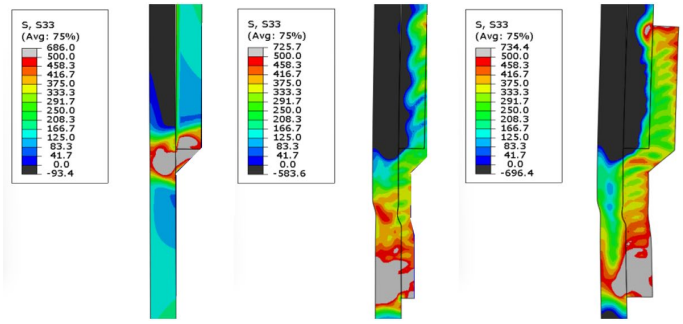

(a) Hoop stress – as-welded sleeve, with small and larger weld overlays

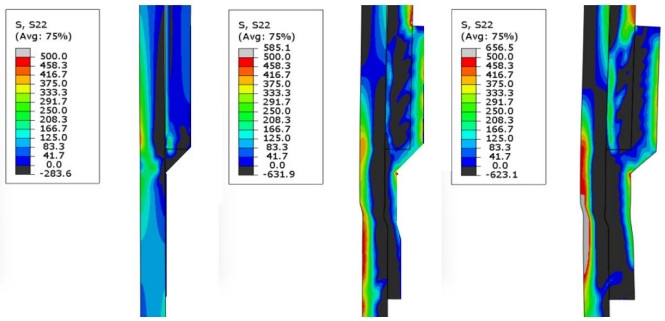

(b) Longitudinal stress – as-welded sleeve, with small and larger weld overlays

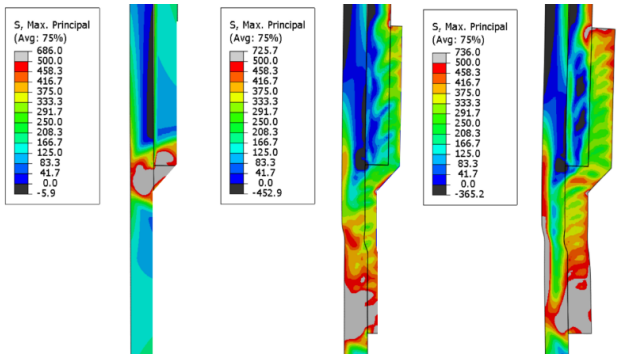

(c) Maximum principal stress

Figure 9 Weld residual stresses in Type B repair sleeve assuming pressure through the carrier pipe to the annular gap of the repair sleeve. This was for a steady-state welding region (no start-stop locations), and weld sequencing from top to bottom (from sleeve towards carrier pipe, or top to bottom in above depictions) – stress scales are in MPa.

A further effort was conducted using the half-thickness weld overlay, but in this case the weld repair was made from the carrier pipe (bottom of the figures) towards the center of the repair sleeve, see Figure 10. In this case, the higher principal stresses changed from being in the carrier pipe to being in the sleeve. This is a more desirable weld sequencing since the carrier pipe stresses are not affected significantly. Having higher residual stresses in the center of the repair sleeve is not a concern since there are no flaws there like there could be in the fillet weld.

Obviously there could be more optimizing for an actual repair procedure. But should an operating blended-hydrogen pipeline ever need to have a defective area repaired where a pressure containing sleeve is needed, this type of approach is an option.

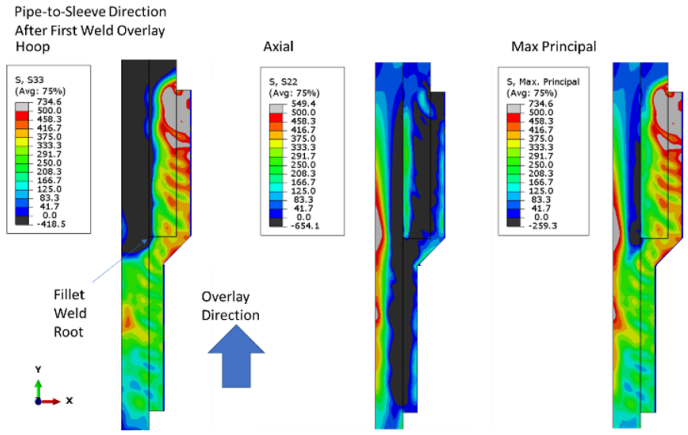

Figure 10 Sensitivity study with reversing the weld sequencing of the overlay on top of the fillet weld region

Task 5 – Assess Critical Flaw Sizes and Respective Detection Thresholds

The efforts in this task are undertaken in two different approaches. The first is the development of fundamental aspects of hydrogen diffusion in steels under the influence of stress and plastic deformation and the resulting effects on damage progression and fracture toughness being undertaken with the significant assistance of Professor Xiaosheng Gao of the Department of Mechanical Engineering of the University of Akron. This is a longer-term developmental effort that will eventually be needed to assess some complex geometries such as the potential effects of hydrogen on: weld defects in type B repair sleeves, hydrogen injection nozzle saddle welds, dents, gouges, wrinkle bends, etc. The fundamental aspects are first being developed by Prof Gao, while Emc^2 staff will utilize the computational developments for these more complex but pragmatic geometries. Subtask 5.1 describes those efforts.

The second approach is to provide some near-term pragmatic guidance for cases with and without hydrogen such as axial cracks in pipes and crack severity within hard spots. These on-going efforts are described in Subtask 5.2.

In a parallel DOT/PHMSA project (693JK32210013POTA) on *Reviewing of Integrity Threat Characterization Resulting from Hydrogen Gas Pipeline Service* also at Emc^2, we are tasked to develop a 5-year field-testing plan to validate integrity-management challenges. The work in all of Task 5 is valuable input to that effort as well.

Subtask 5.1 - Hydrogen Diffusion in Steels under the Influence of Stress and Plastic Deformation and the Resulting Effects on Damage Progression and Fracture Toughness – Development of Fundamental FE Evaluation Methods

The following aspects are discussed in this quarterly report for the initial University of Akron hydrogen diffusion/transport model. The efforts here are to show some of the fundamental aspects and then examine a few initial cases to see their importance. Initially there are some very detailed equations and results that show the different competing mechanisms for hydrogen transport within steels. This is provided for the interested reader, but also to get a grasp of the results for later more pragmatic applications. Later in this section, just some of the final concentration color contour plots results are presented.

1. Hydrogen transport model basic equations
2. Material properties
3. Double-notched specimen
    a. Internal Damage
    b. Environmental/hydrogen damage
4. Dented pipe
    a. No internal pressure
    b. With internal pressure
5. HELP effect
6. Discussions
7. Conclusions

1. Hydrogen Transport Model

Hydrogen is assumed to reside either at normal interstitial lattice sites (NILS) or trapping sites generated by plastic straining by the following equation.

$$C = C_L + C_T = \theta_L N_L + \theta_T N_T$$

Where:

C_T: hydrogen concentration per unit volume in trapping sites
C_L: hydrogen concentration in NILS
θ_L: occupancy of the NILS
θ_T: occupancy of the trapping sites
N_L: # of solvent lattice atoms per unit lattice volume
N_T: trap density, N_T (ε_p)

The two populations are assumed to be in equilibrium according to Oriani's theory, and the relationship between θ_L and θ_T is

$$\frac{\theta_T}{1-\theta_T} = \frac{\theta_L}{1-\theta_L} exp\left(\frac{W_B}{R\Theta}\right)$$

Where:

W_B: trap binding energy,
R: universal gas constant, *and*
Θ: absolute temperature.

The diffusion process occurs through transposition between interstitial sites within the lattice. Elastic lattice expansion due to hydrostatic stress increases the solubility for atomic hydrogen whereas inhomogeneities due to dislocations act as traps. The governing equation for transient hydrogen diffusion is

$$\frac{C_{\mathrm{L}} + C_{\mathrm{T}}(1-\theta_{\mathrm{T}})}{C_{\mathrm{L}}}\frac{\partial C_{\mathrm{L}}}{\partial t} - \nabla(D_{\mathrm{L}}\nabla C_{\mathrm{L}}) + \nabla\left(\frac{D_{\mathrm{L}}C_{\mathrm{L}}V_{\mathrm{H}}}{R\Theta}\nabla\sigma_{\mathrm{h}}\right) + \theta_{\mathrm{T}}\frac{\mathrm{d}N_{\mathrm{T}}}{\mathrm{d}\varepsilon_p}\frac{\partial\varepsilon_p}{\partial t} = 0$$

Where:

D_{L}: hydrogen diffusion coefficient through NILS,
V_{H}: partial molar volume of hydrogen, and
σ_{h}: hydrostatic stress.

In the presence of hydrogen, the hydrogen-induced lattice deformation needs to be included, which is purely dilatational. Therefore, the total deformation rate should consist of an elastic part, a plastic part and a part due to lattice straining by the solute hydrogen per the below equation.

$$D_{ij} = D_{ij}^{e} + D_{ij}^{p} + D_{ij}^{h}$$

The equivalent plastic strain is calculated as,

$$\varepsilon_p = \int \sqrt{\frac{2}{3}D_{ij}^{p}D_{ij}^{p}}\,\mathrm{d}t$$

2. Material Properties

The material considered is a X52 steel with a Young's modulus of 200 GPa and Poisson's ratio of 0.3. The tensile curve in terms of stress versus plastic strain is given in the below figure.

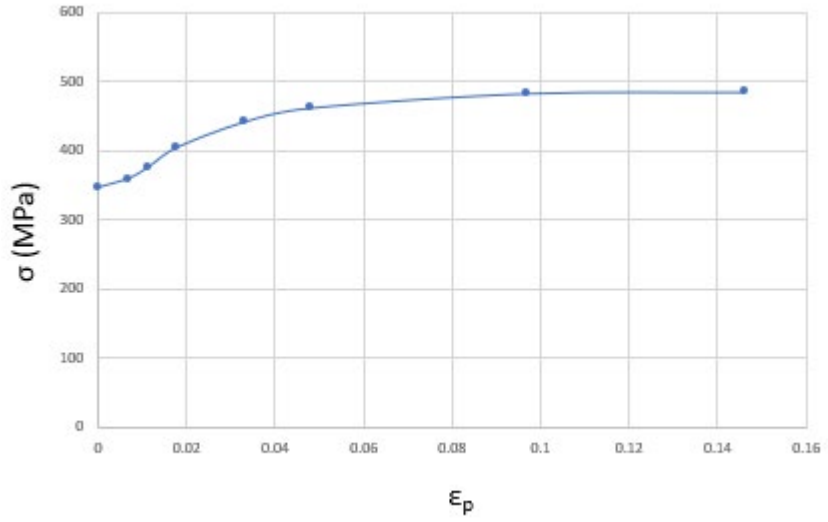

Figure 11 Stress versus plastic-strain curve for X52 steel in this study

Other material properties are taken from Taha and Sofronis (2001) and listed in Table 1.

Table 1 Other material property values used for hydrogen diffusion evaluation

Properties	Values	Units
Molar volume of iron	$V_M = 7160$	mm^3/mol
Lattice site density	$N_L = 8.46 \times 10^{19}$	$atoms/mm^3$
Molar volume of hydrogen in solid solution	$V_H = 2000$	mm^3/mol
Binding energy	$W_B = 60$	kJ/mol
Number of NILS per solvent atom	$\beta_L = 6$	-
Number of sites per trap	$\beta_T = 1$	-

The trap density for iron and steels is given as a function of local effective plastic strain.

$$\log(N_T) = 23.26 - 2.33\exp(-5.5\varepsilon_p)$$

The diffusion coefficient and initial hydrogen concentration used in most literature are D_L = 0.0127 mm^2/s and 2.084×10^{12} $atoms/mm^3$, respectively. However, the initial Emc^2 calculations used much larger values in those analyses, i.e., D_L = 3,600 mm^2/s and C_0 = 2.5 ppm (corresponding to 1.18×10^{16} $atoms/mm^3$). Both sets of parameters are considered in the analyses presented in this report.

3. Double-notched tension specimen with offset notches

This study was conducted to assess the internal hydrogen absorption in a specimen that had high shear stress as well as localized triaxial tension stress, which is a fundamental test of the theory. The following inputs were used:

- Initial surface hydrogen concentration (uniform C_{L0}): 2.084×10^{12} $atoms/mm^3$
- Diffusion coefficient (D_L): 0.0127 mm^2/s
- Outer edges of the specimen: insulated
- Loading: 0.2-mm displacement on top edge is applied in 10^6 seconds (quasi-static, steady state)

The finite element mesh and dimensions are shown in Figure 12.

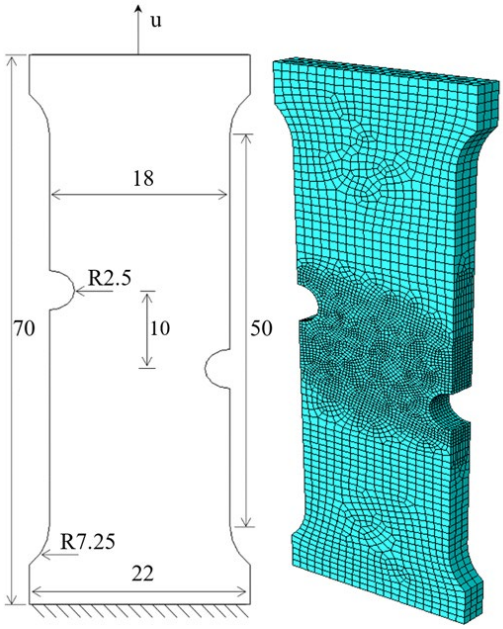

Figure 12 Finite element model of initial offset double-edge notched specimen (Dimensions in mm)

The final steady-state hydrogen distribution is shown on the surface and at the mid-thickness plane in Figure 13, while the various parameters used to get the total hydrogen concentration are shown in Figure 14 and Figure 15.

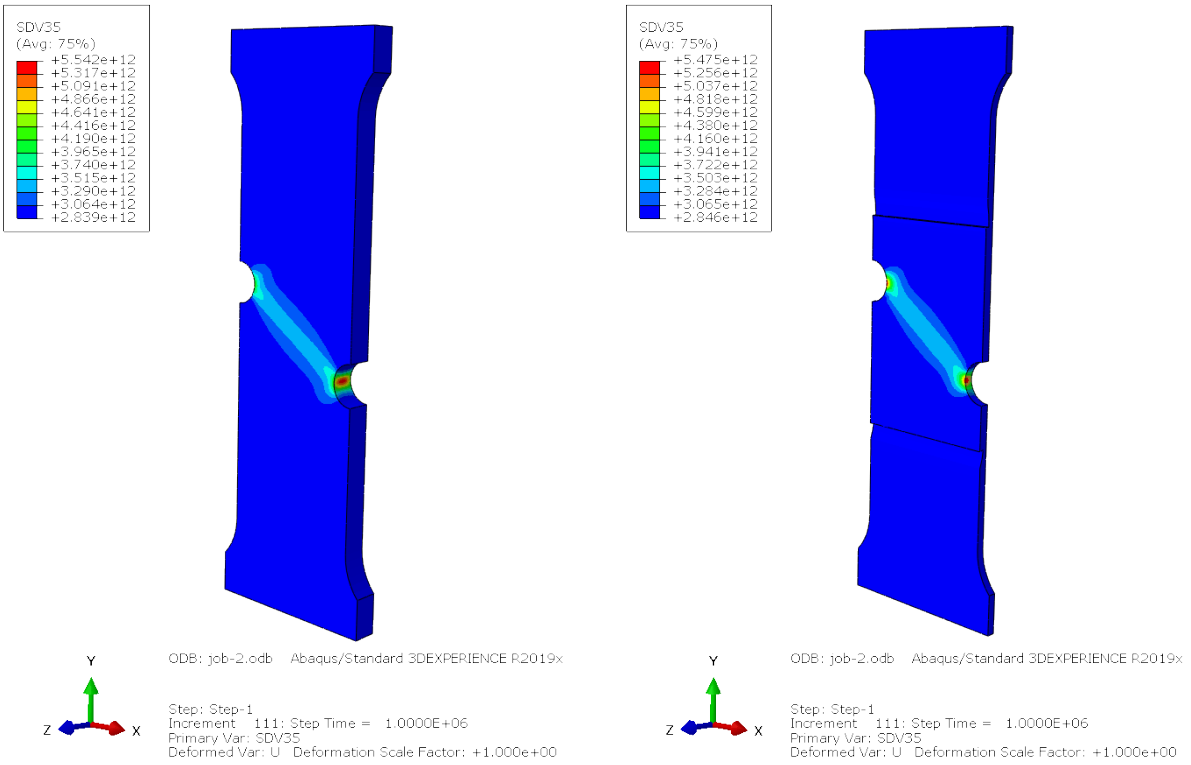

(a) C_{total} on the surface (b) C_{total} in the mid-thickness plane

Figure 13 Total hydrogen distribution ($C_{total} = C_T + C_L$) for this trial case

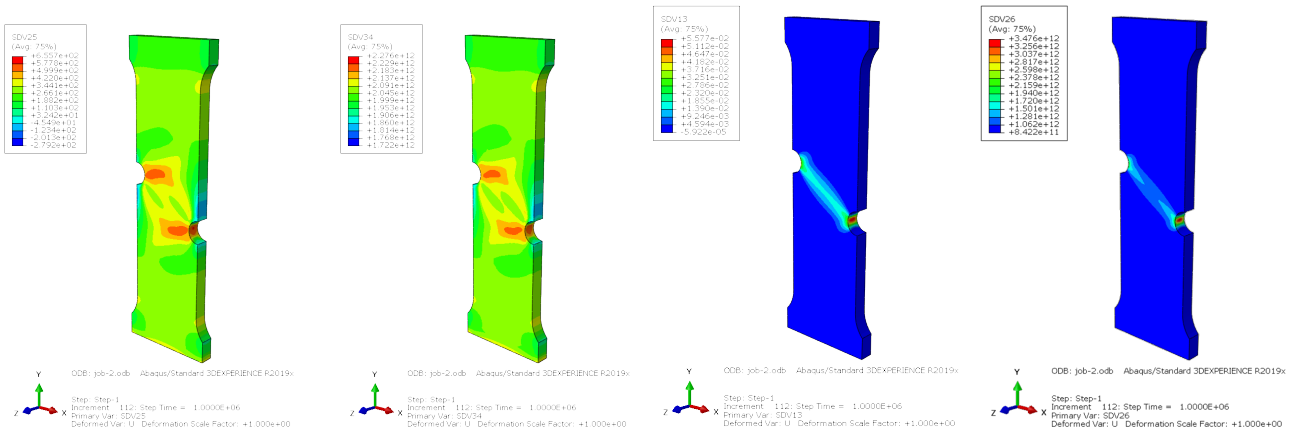

(a) σ_{kk} ($3\sigma_h$) **(b) C_L** **(c) ε_p** **(d) C_T**

Figure 14 Surface values of various calculated parameters; (a) hydrostatic stress level, (b) hydrogen concentration in normal interstitial sites, (c) equivalent plastic strain, and (d) hydrogen concentration per unit volume in trapping sites

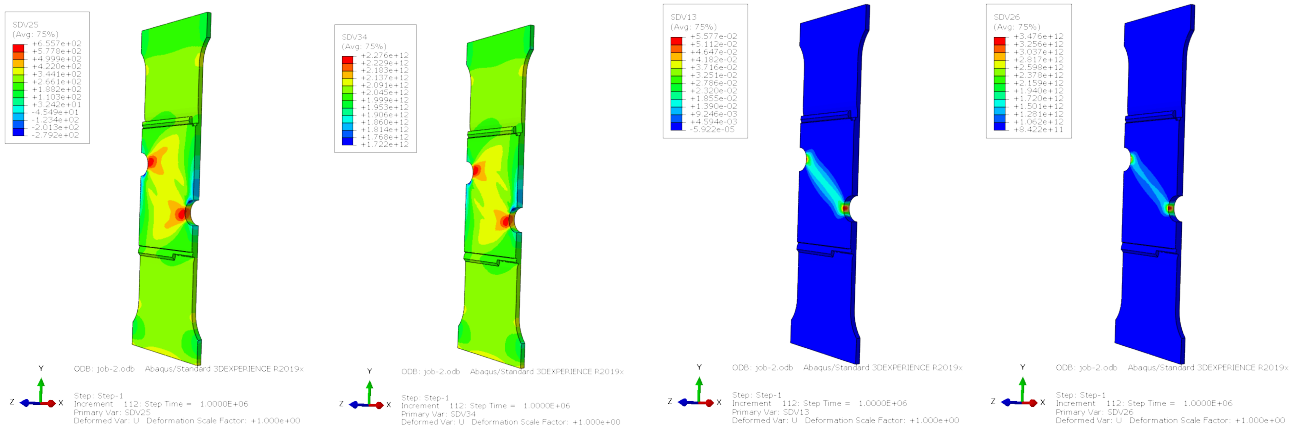

(a) σ_{kk} ($3\sigma_h$) (b) C_L (c) ε_p (d) C_T

Figure 15 Mid-thickness plane values of various parameters; (a) hydrostatic stress level, (b) hydrogen concentration in normal interstitial sites, (c) equivalent plastic strain, and (d) hydrogen concentration per unit volume in trapping sites

From this initial evaluation, one can see the different concentration components (C_L and C_T) vary in shape and spatial location due to the hydrostatic stress and plastic strain distributions. The C_T concentration was the dominant component to the total hydrogen concentration.

4. Dented Pipe

The 2-dimensional modelling of a dented pipe was one of the original Emc^2 sensitivity studies to assess hydrogen concentration in pragmatic pipe integrity challenges. The following analysis compared the built-in capability in ABAQUS to the more advanced hydrogen diffusion analyses being pursued. The pipe is first allowed to absorb hydrogen, then it is indented, the indenter is then removed. Finally, the hydrogen concentration is allowed to reach the steady-state condition. The first set of analyses is with no internal pressure then repeated with internal pressure.

Dented Pipe Without Internal Pressure

The pipe being modelled has a 36-inch (914.4 mm) outside diameter and 0.39-inch (9.9 mm) wall thickness X52, typical of a vintage linepipe. The head of the indenter is circular with a radius of 2 inches (50 mm). The steps and other input parameters were.

- No internal pressure initially
  - Initial hydrogen concentration: 0
  - Hydrogen concentration at ID: $C_L = 2.084 \times 10^{12}$ atoms/mm^3
  - Hydrogen concentration at OD: $C_L = 0$
  - Diffusion coefficient (D_L): 0.0127 mm^2/second
- Step 1: hydrogen diffusion to reach steady state (10^6 seconds)
- Step 2: indentation of 120 mm (100 seconds)
- Step 3: release of indenter (100 seconds)
- Step 4: Steady-state hydrogen distribution (10^6 seconds)

At end of Step 3

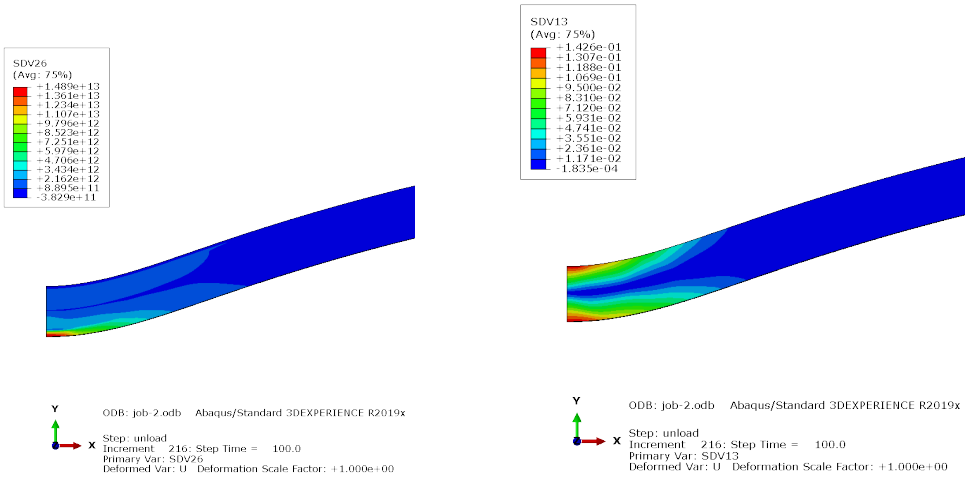

(a) σ_{kk} $(3\sigma_h)$ (b) ε_p

Final steady-state

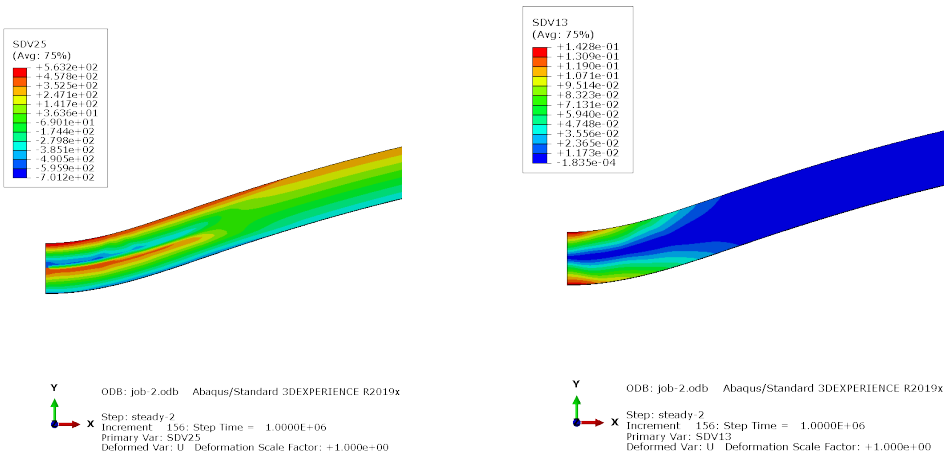

(c) σ_{kk} $(3\sigma_h)$ (d) ε_p

Figure 16 Changes in hydrostatic stress and plastic strain from release of indenter to steady-state condition

At end of Step 3

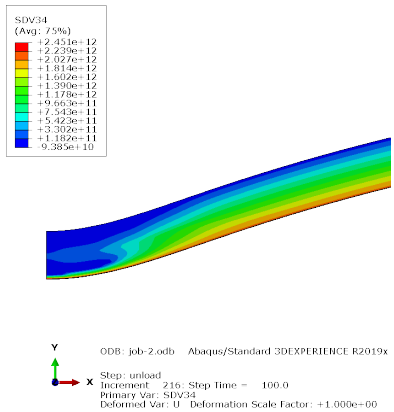

(a) C_L

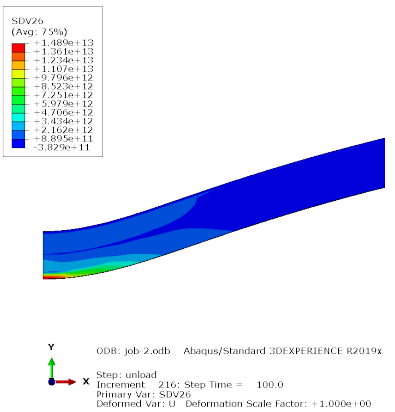

(b) C_T

Final steady-state

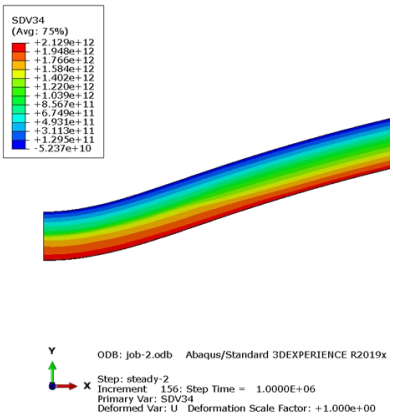

(c) C_L

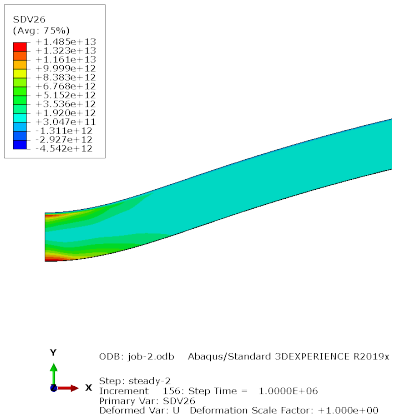

(d) C_T

Figure 17 Changes in C_T (hydrogen concentration per unit volume in trapping sites) and C_L (hydrogen concentration in normal interstitial sites) contributions from release of indenter to steady-state condition

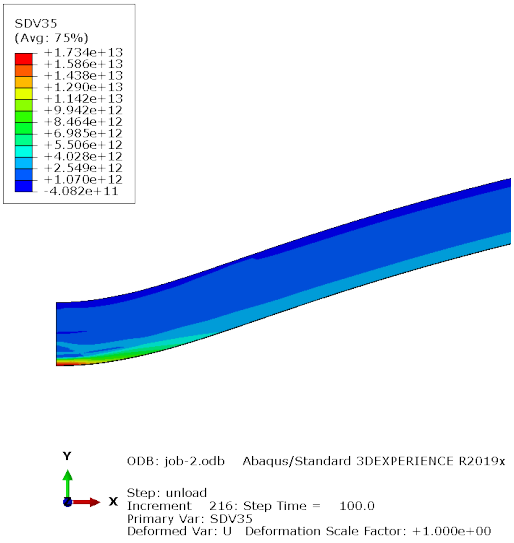

(a) At release of indenter

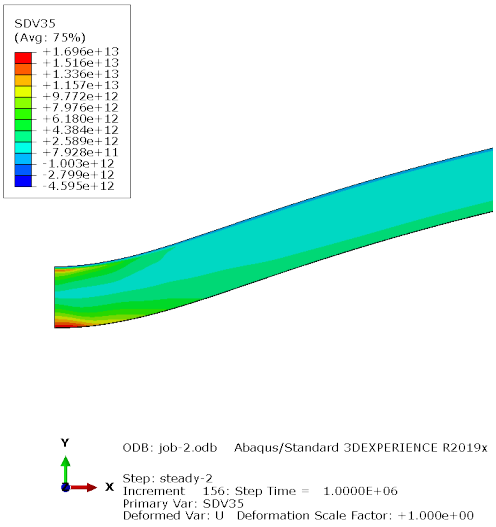

(b) at steady state absorption time

Figure 18 Change in total concentration of hydrogen from release of indenter to steady-state absorption time (No internal pressure applied)

The following evaluation was done with the initial Emc^2 assumed hydrogen exposure on the inside surface of the pipe to replicate the earlier Emc^2 initial sensitivity study. As with the prior 2D dented pipe evaluation, the pipe is first allowed to absorb hydrogen, then it is indented, the indenter is then removed, then the hydrogen concentration is allowed to reach the steady-state condition.

- No internal pressure
  - Initial hydrogen concentration: 0
  - Hydrogen concentration at ID: $C_L = 1.18\text{x}10^{16}$ atoms/mm^3 (2.5 ppm)
  - Hydrogen concentration at OD: $C_L = 0$
  - Diffusion coefficient (D_L): 3600 mm^2/s
- Step 1: hydrogen diffusion to reach steady state (10^6 s)
- Step 2: indentation of 120 mm (100 s)
- Step 3: release of indenter (100s)
- Step 3: Steady-state hydrogen distribution (10^6 s)

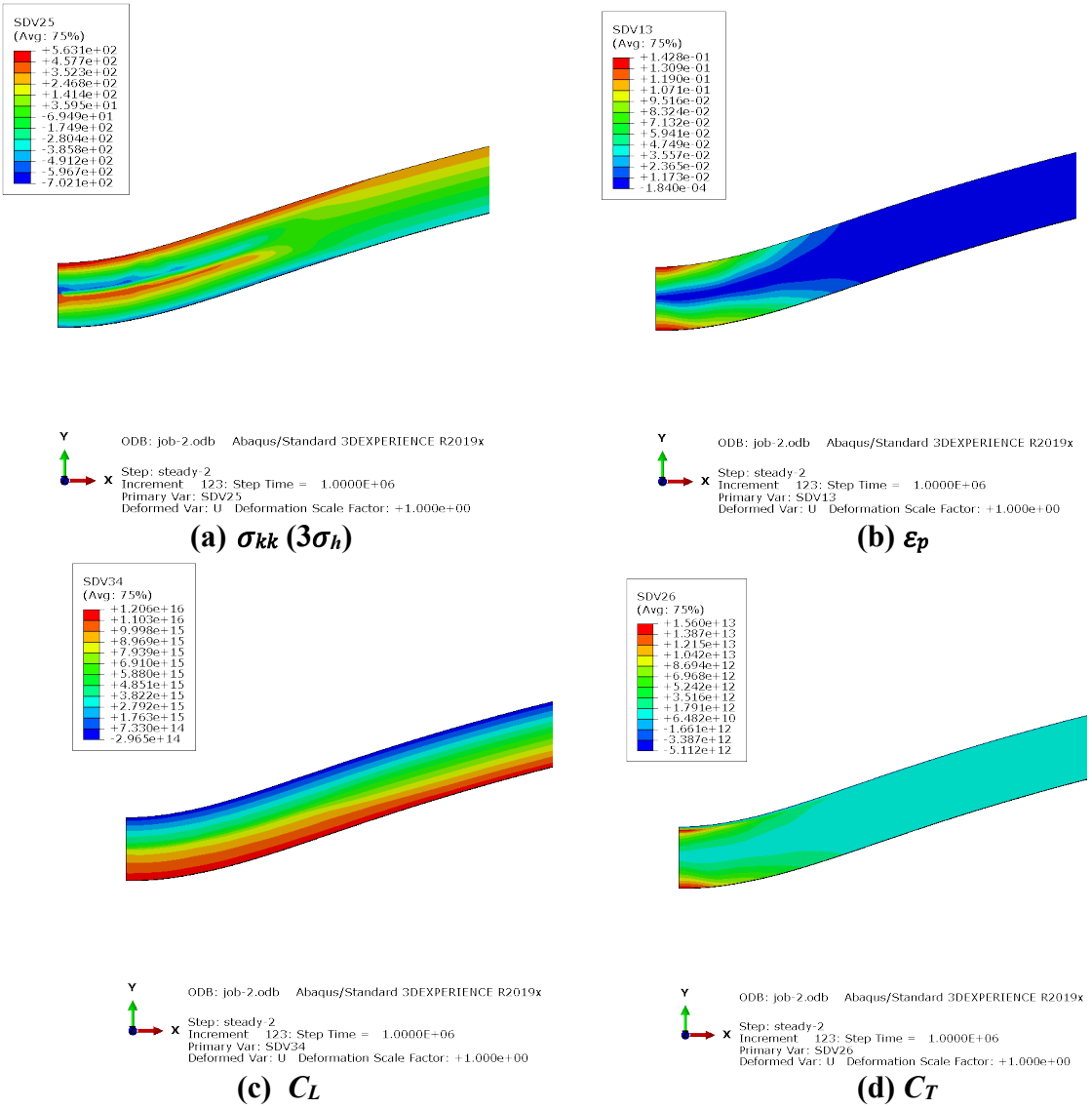

Figure 19 The final steady state values of the; hydrostatic stress [σ_{kk} ($3\sigma_h$)], plastic strain (ε_p), C_L (hydrogen concentration in normal interstitial sites), and C_T (hydrogen concentration per unit volume in trapping sites) (No internal pressure applied)

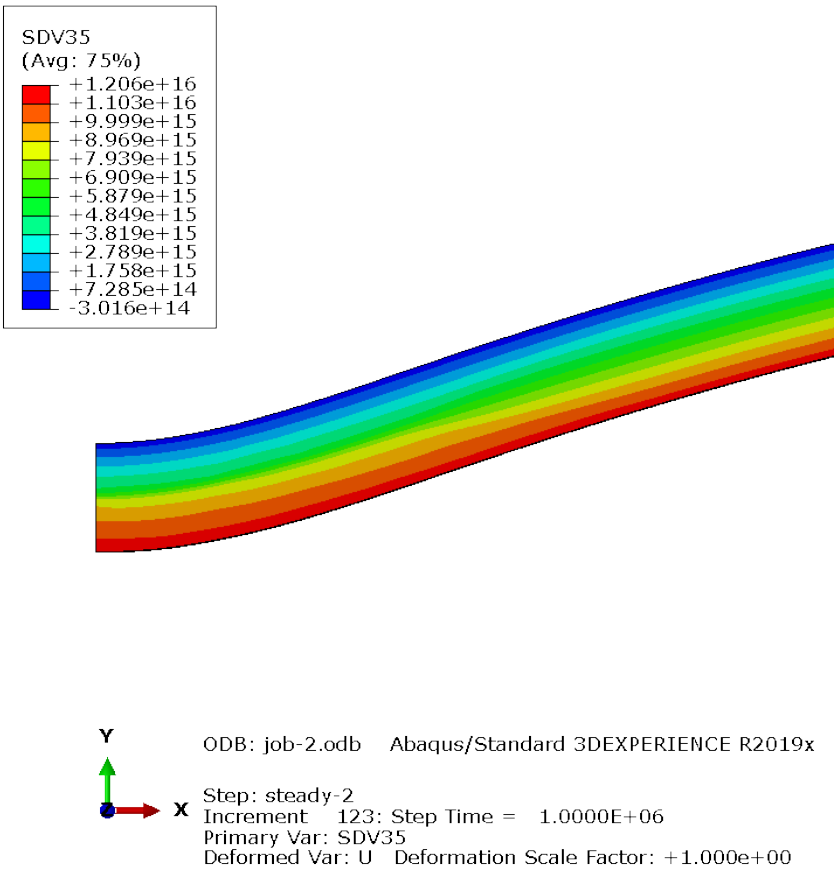

Figure 20 Final steady-state total hydrogen concentration (C_{total}) for the 2D dent case using the University of Akron diffusion model (No internal pressure applied)

In the dented pipe model without internal pressure, $\nabla\sigma_h$ is not high enough such that ε_p becomes the dominant factor affecting the hydrogen distribution. Consequently, the hydrogen concentration is highest at ID in the dented area where ε_p is largest.

Dented Pipe with Internal Pressure

The next step was to apply the internal pressure of 5.592 MPa (811 psig), and then go through the same indention procedure. This was first done with the hydrogen concentration at ID of $c_o = 2.084\text{x}10^{12}$ atoms/mm^3, and the diffusion coefficient (D_L) of 0.0127 mm^2/s; then repeated with hydrogen concentration at ID of $c_o = 1.18\text{x}10^{16}$ atoms/mm^3 (2.5 ppm), and the diffusion coefficient (D_L) of 3600 mm^2/s. The latter case being the original Emc^2 sensitivity case with the built-in ABAQUS capability. All other steps were identical to the unpressurized pipe denting analysis.

Rather than showing all the parameters and intermediate steps, only the final total hydrogen concentrations are shown in Figure 21.

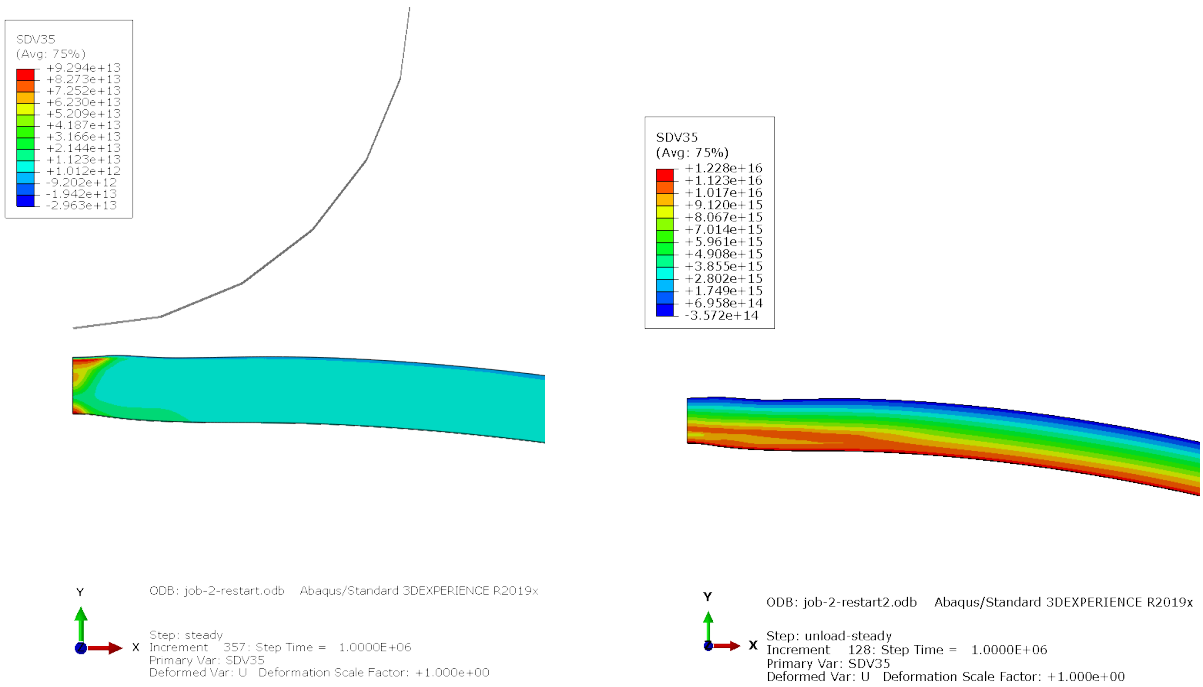

(a) Using c_o = 2.084x10^{12}, D_L=0.0127 mm^2/s **(b) Using c_o = 1.18x10^{16}, D_L=3600 mm^2/s**

Figure 21 Comparison of total hydrogen concentration at dented pipe after pressure applied and reaching steady-state conditions

For the dented pipe with internal pressure, $\nabla\sigma_h$ in the region near the centerline of wall thickness is large enough to cause noticeable increase of C_L. For the case of low diffusivity and low hydrogen concentration at ID, C_L is still larger than C_T in the dented area, so the total hydrogen concentration is dominated by C_T. But for the case of high diffusivity and high hydrogen concentration at ID, C_L becomes the dominant factor in the dented area, so the hydrogen concentrations in these two cases look drastically different because of the C_L versus C_T dominance. *Understanding this trend can be important for blended hydrogen lines that might start with low blend ratios, i.e., less than 5%, but then increase to higher ratios of 20% or greater.*

5. Incorporating HELP Effect

It has been shown that the presence of hydrogen in solid solution decreases the barriers to dislocation motion, and thus increases the amount of plastic deformation in a localized region adjacent to fracture surface or high stressed regions. Sofronis et al. proposed a simple model to describe the HELP effect by reducing the yield stress with the increase of hydrogen concentration as given below.

$$\sigma_0(c) = f(c)\,\sigma_0$$

$$f(c) = \begin{cases} (\xi - 1)\dfrac{c}{c_0} + 1 & f(c) > \eta \\ \eta & f(c) \le \eta \end{cases}$$

Where c is the hydrogen concentration, σ_o is the yield stress with no presence of hydrogen, ξ is a softening parameter defining the yield stress when the hydrogen concentration equals to c_o, and η η defines the lowest possible value of yield stress (minimum yield strength) from the hydrogen.

In the results presented in this section, the values of ξ and η are taken as 0.99 and 0.85 respectively. First the double-notched specimen analyzed (internal hydrogen absorption) is reanalyzed, where the HELP effect is included in the analysis. The results are in the below figure for the final hydrogen distribution on the surface.

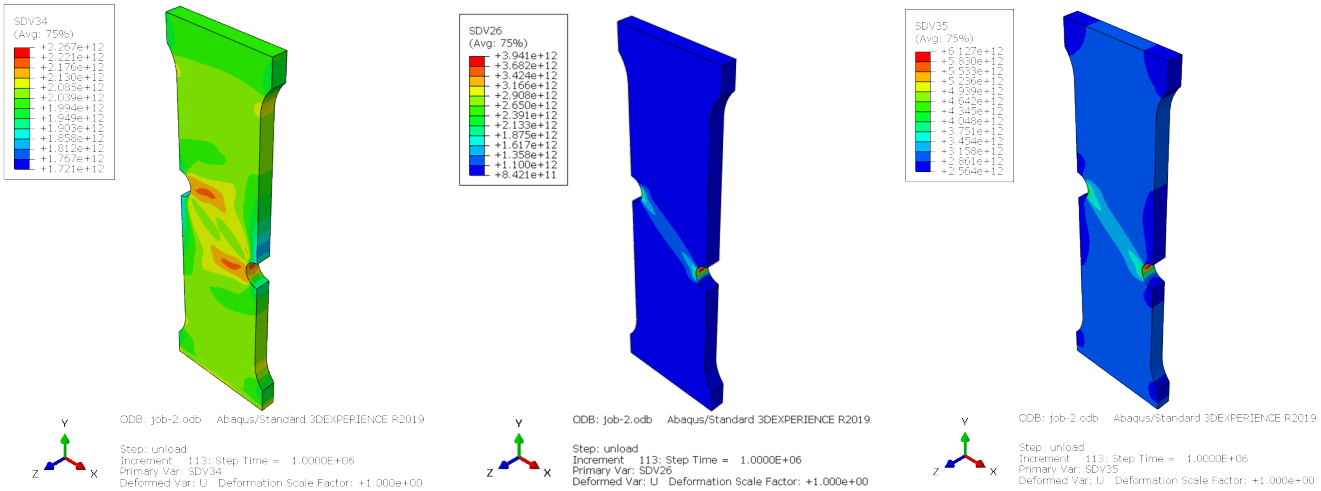

(a) C_L **(b) C_T** **(c) C_{total}**

Figure 22 Double-edge notched tension specimen using the HELP effect to reassess the total hydrogen concentration (C_{total})

With the HELP effect considered, more trapping sites are available so that the contribution of C_T to the total hydrogen concentration is further increased (compared to Figure 13 values), peak value of 6.17e+12 atoms/mm^3 vs 5.69e+12 atoms/mm^3.

6. Discussion

The initial Emc^2 analysis of the dented pipe model used the extended Fick's law provided by ABAQUS, which includes the effect of the pressure (hydrostatic stress) gradient. For uniform temperature, the ABAQUS model compute the concentration flux by

$$\boldsymbol{J} = -s\boldsymbol{D} \cdot \left[\nabla\phi + \kappa_p \nabla p\right]$$

where s is the solubility of the diffusing material in the base material, D is the diffusivity, ϕ is the normalized concentration defined as $\phi = c/s$, c is the mass concentration, κ_p is the pressure stress factor, and $p = -\sigma_h = -\sigma_{kk}/3$.

Assuming isotropic material with D=3.6×10^{-3}m^2/s and κ_p ramping from 0 to 10-6 mN$^{-1/2}$ as c changes from 0 to 150 ppm, the initial Emc^2 calculations found that for the case of dented pipe without internal pressure, the steady-state hydrogen concentration is highest near the centerline of the wall thickness where the hydrostatic stress ($-p$) is the highest.

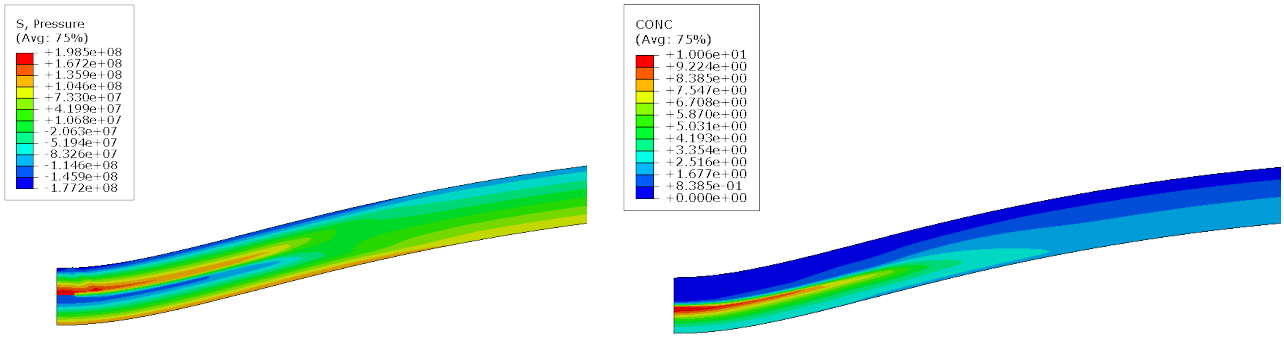

(a) P ($-\sigma_h$) **(b) Total concentration**

Figure 23 Emc²'s ABAQUS results for hydrostatic pressure and predicted hydrogen concentration

In the University of Akron hydrogen transport model being pursued in this project, the hydrogen flux is given by

$$\boldsymbol{J} = -D_L \nabla C_L + \frac{D_L C_L V_H}{R\theta} \nabla \sigma_h$$

The effect of hydrostatic stress gradient is determined by the physical parameters. With the given values of these parameters, the hydrostatic stress gradient near the centerline is not high enough to cause noticeable change of C_L distribution in this area. However, if we artificially increase the factor before $\nabla\sigma_h$ by 10 times, the C_L distribution would become the following, where the increase in C_L near the centerline is more pronounced, see Figure 24.

The ABAQUS built-in model does not take into account the hydrogen atoms going to the trapping sites generated by plastic deformation (C_T), and hence will not be able to accurately predict hydrogen distribution in plastically deformed structures. This will be important for welds, dents, wrinkle bends, etc. where there are plastic deformed regions. The reliability of the predicted hydrostatic stress effect computed by the ABAQUS built-in model depends on how accurate the κ_p factor is prescribed.

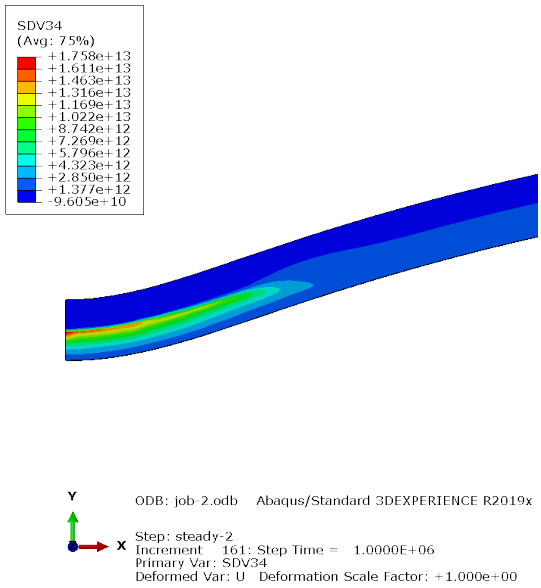

Figure 24 University of Akron model result obtained by artificially increasing the factor before $\nabla\sigma_h$ by 10 times

7. Conclusions

The following conclusions can be drawn from the analysis results:

1. Hydrogen concentration in material comes from the combined contributions of hydrogen at normal interstitial lattice sites, NILS, (C_L) and hydrogen at trapping sites (C_T).
2. C_L is driven by the hydrostatic stress gradient ($\nabla\sigma_h$), while C_T is controlled by the plastic strain (ε_p).
3. In the double-notched specimen, near notch tips, both $\nabla\sigma_h$ and ε_p are high, and thus hydrogen tends to accumulate in these regions.
4. In the dented-pipe model without internal pressure, $\nabla\sigma_h$ is not high enough such that ε_p becomes the dominant factor affecting the hydrogen distribution. Consequently, hydrogen concentration is highest at ID in the dented area where ε_p is largest.
5. For the dented pipe with internal pressure, $\nabla\sigma_h$ in the region near centerline of wall thickness is large enough to cause noticeable increase of C_L. For the case of low diffusivity and low hydrogen concentration at ID, C_L is still larger than C_T in the dented area, and the total hydrogen concentration is dominated by C_T. But for the case of high diffusivity and high hydrogen concentration at ID, C_L becomes the dominant factor in the dented area. *This different behavior can be important as hydrogen blended pipeline increases the percent of hydrogen in the gas.*
6. With the HELP effect used, more trapping sites are available so that the contribution of C_T to the total hydrogen concentration is further increased.
7. The reliability of the predicted hydrostatic stress effect computed by the ABAQUS built-in model depends on how accurate the κ_p factor is prescribed.
8. The ABAQUS built-in model does not take into account the hydrogen atoms going to the trapping sites generated by plastic deformation (C_T) and will not be able to accurately predict hydrogen distribution in plastically deformed structures.

This last factor will be highly important for welds, dents, wrinkle bends, etc. where there are plastic deformed regions, so the initial study results are of high general value.

Subtask 5.2 Near-Term Critical Flaw Size Evaluations

For the purposes of understanding the potential impact of hydrogen degradation on the critical flaw sizes for structure integrity of hydrogen pipelines, some sensitivity studies are underway. These results will be used as guidance to determine if additional efforts in that integrity threat area are needed and see what industry has planned to address those aspects.

The two initial evaluations being conducted in this subtask are (1) the changes in the critical flaw sizes for axial surface cracks due to hydrogen degradation of the upper-shelf toughness of the steels, and (2) how the critical crack sizes might change in a hardspot. There are two quite different analyses approaches for these evaluations as described below.

Changes in Axial Surface Crack Critical Flaw Sizes

Earlier work at Battelle, and more recent work by Sandia (and others) have shown that linepipe steel toughness decreases at room temperature with hydrogen exposure when using standard compact-tension, C(T), specimens. There is not a definitive result yet to show if more borderline linepipe welds (i.e., LF-ERW weld fusion lines) have a shift in the brittle-to-ductile transition temperature due to hydrogen uptake, i.e., is there really hydrogen "embrittlement". So, the following study is being limited to upper-shelf toughness changes on the critical flaw sizes, which is probably sufficient for base metals, but maybe not some of the LF-ERW vintage pipe with higher carbon content and much warmer transition temperatures for a pipe with a surface crack.

The determination of the burst pressure, or critical flaw sizes at a given pressure, is traditionally done with several older empirical analyses that use the Charpy impact energy as a measure of the toughness. In hydrogen, the higher loading rate in Charpy testing has little effect on the impact energy (with a few exceptions). Hence analysis procedures are needed that use fracture mechanics tests like the C(T) specimen testing. But it is also known that the standard C(T) specimen is a conservative toughness measure due to the bending loading applied. Surface-cracked pipe has the ligament loaded more in tension, which results in a higher toughness. A single-edge-notch-tension, SEN(T), specimen behaves more like a surface crack since they have similar constraint conditions. Furthermore, the SEN(T) and surface-cracked pipe show that the toughness changes with the crack depth [a/t in the pipe or a/w in the SEN(T)]. Figure 25 shows the general relationship between C(T) specimen toughness and SEN(T) specimens, where the C(T) test has a standard crack length to width ratio (a/w) of about 0.5, while the a/w in the SEN(T) can be varied. So, we must take the hydrogen toughness data from C(T) testing and make constraint corrections, so it is applicable to surface cracks in pipe.

At a given pressure, there can be a combination of axial surface crack depths with lengths that could all fail at the same burst pressure. This is illustrated in Figure 26 using the older Original Ln-Sec equation (based on empirical fits with Charpy energy). In this figure, the line for the operating pressure crosses the curves for the surface crack failure pressure at different crack lengths for each surface crack depth/thickness ratio (a/t). Hence in a burst pressure predictive analysis that uses fracture toughness data from hydrogen testing, the toughness needs to change as a function of a/t, as per the discussion in the prior paragraph.

Various axial surface-cracked pipe burst pressure analyses are being evaluated as part of a different DOT/PHMSA project at Emc^2, *693JK32010010POTA - Hydrostatic Retesting Optimization for Older Liquid Pipelines.* Of the analyses being examined, the one that is probably the most accurate is the

2022IPC FE/J-estimation procedure developed at Emc^2 for that project. The spreadsheet analysis that has that analysis procedure is in the process of updated, as well as the other analyses such as the Original Ln-Sec, the Modified Ln-Sec, CorLAS, API-579 FAD approach, and PRCI MAT-8. The constraint procedure to go from C(T) specimen to toughness as a function of a/t as shown in Figure 25 is being automated. Some examples of how the toughness changes with hydrogen (using J-R curves where the toughness also changes with crack growth) are shown in Figure 27 where much more data is compiled from the literature review in Task 1.

The QA of the final spreadsheet is in progress, and calculations should be started in July 2023.

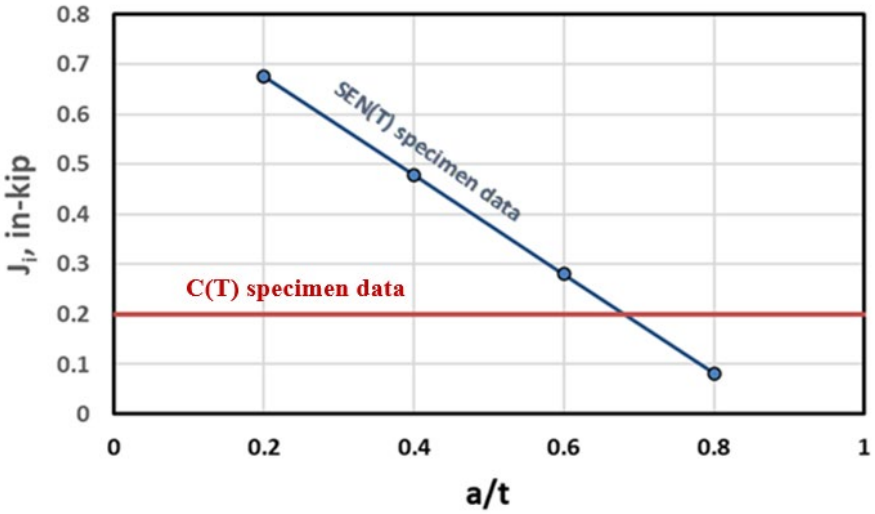

Figure 25 Comparison of crack initiation toughness values (J_i) from C(T) versus SEN(T) specimens for a vintage line pipe steel

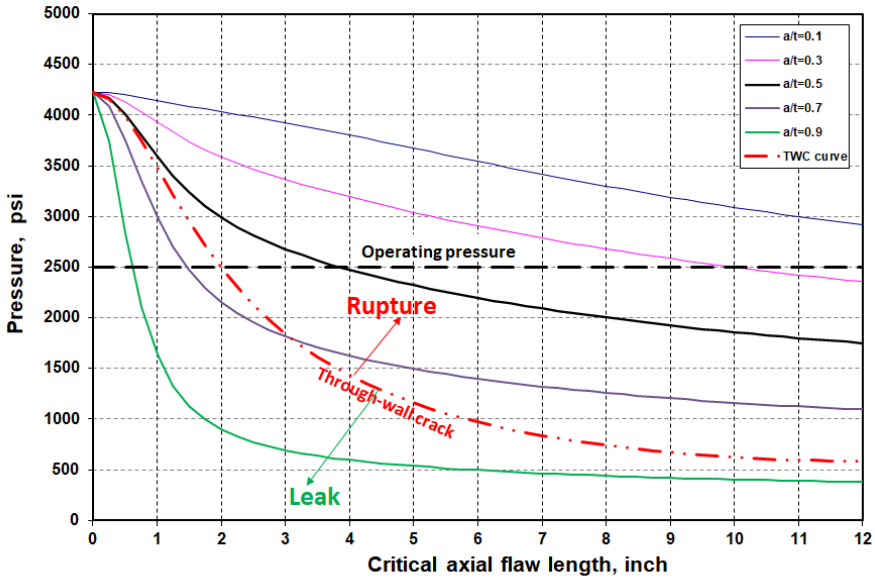

Figure 26 Example graph of burst pressure prediction results for axial crack in a pipe using the Original Ln-Sec equation

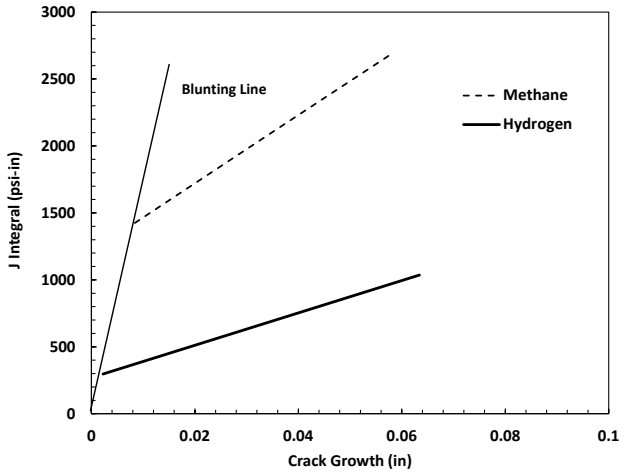

(a) 1980 vintage X70 steel

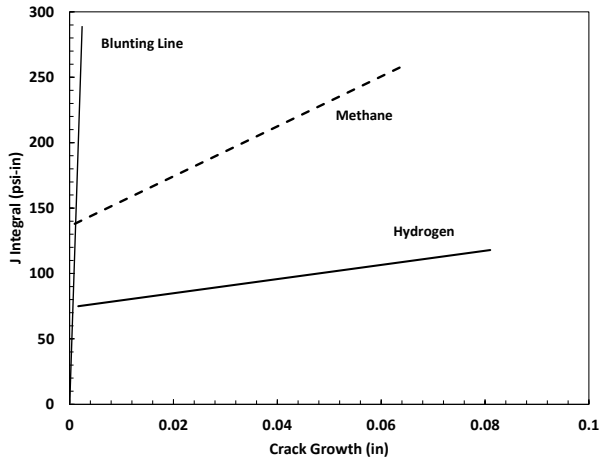

(b) Pre-1960 X42 linepipe base metal heat-treated to represent a hard spot

Figure 27 Examples of how the J-R curve of linepipe materials can change with hydrogen exposure

Changes in Critical Crack Sizes in Hard Spots

Hard spots are of particular interest since there have been some failures in natural gas service with hard spots, where there was a combination of coating loss, higher pH soil, and the cathodic protection (CP) may have been too high. These conditions were believed to cause hydrogen charging of the material from outside conditions. Typically, such hard spot failures are in older lines from local unintended overcooling when the plates were in the red-hot (fully austenitized) condition. The concern for pipe that will transport blended hydrogen is that the coating need not be missing, and CP anomalies may need not cause other well protected hard spots to fail even with good external environmental protection.

The sensitivity study being undertaken in this project involves trying to incorporate several aspects of the pipe with hard spots that simple axial surface-cracked pipe analyses cannot handle. To understand these different facets, the whole pipe fabrication process is first reviewed to understand the loading conditions that should be applied.

The starting point is having a plate in a rolling mill that is at red-hot temperature conditions. At this temperature the microstructure of the steel is austenite. Under normal conditions the plate would cool down in a controlled fashion, and for vintage linepipe material the microstructure would be ferrite/perlite.

For the red-hot plate, there could be an unintended cooling condition in a localized region. The cooling will cause the material to shrink relative to the rest of the red-hot plate, and the microstructure will change to martensite with a mixture of ferrite. Martensite is quite hard compared to the final ferrite/perlite microstructure. Martensite will have a crystal structure that is face-centered tetrahedral (FCT), while the rest of the red-hot plate has a body-centered cubic (BCC) austenitic structure. The specific volume of the FTC is about 8 to 9 percent smaller than the BCC structure. So, there are both thermal shrinkage and phase-transformation shrinkage of the hard spot relative to the red-hot plate. This shrinkage is effectively a tensile strain that pulls on the surrounding red-hot plate. The plate material will be plastically strained and give a resulting residual stress within the hard spot. Later the red-hot plate cools and transforms to FCC ferrite/pearlite, so that phase transformation strain is

eliminated, although there is still the plastic straining from the thermal process. Once at room temperature then there is a redistribution of stresses in the hard spot region. So, the initial loading on the hard spot is from the residual stresses of creating the hard spot when it is in plate form.

The plate is then taken to the pipe mill and is fabricated into pipe. This operation is done at ambient temperatures, so there is cold working/straining of the plate material. From an older PRCI/NG-18 project report, this pipe fabrication is typically a through-thickness bending stress of about 10 ksi, in tension on the OD and compression on the ID. However, the hard spot is stronger, and the rest of the pipe deforms around the hard spot during the pipe fabrication process. This is why hard spots also have flat regions. So, the pipe fabrication process needs to be included in the applied stresses, but a flat region of the hard spot may also be important. The flat region may experience more through-thickness bending when the pipe is pressurized, giving additional tension on the OD surface where a hydrogen crack can form.

Hence the loading on the hard spot comes from:

- The thermal and phase transformation shrinkage strain of the hard spot when the rest of the plate is red-hot. This procedure is somewhat akin to a welding residual stress analysis.
- The plate-to-pipe fabrication stresses from the pipe manufacturing.
- Pressure stresses, which may also add a bending stress through the thickness in the flat-hardspot region.

Although Emc^2 also has world-class weld residual stress modeling capabilities to track the weld metal from liquid state to final solid condition in a weld, using weld bead by weld bead travelling arc simulation, the initial study is first simplified by assuming that there is a residual strain in the hard spot that the rest of the pipe resists, and the residual stresses are solved for by finite element (FE) analyses.

In this project, a FE meshing generator has been developed that can make a numerical model of a pipe with any diameter and thickness, a hardspot of any diameter, the hard spot is flat, any external axial surface crack depth and length can be put in the center of the hardspot, and the material properties in the hard spot and rest of the pipe can be defined separately as needed. With the circular hard spot and the axial surface crack centered in the hardspot, the FE mesh can be ¼ symmetry and is shown in Figure 28 with initial preliminary results. The QA of the FE modelling is in progress. Once that is done, then analyses of a matrix of surface cracks with different depths and lengths will be conducted where the toughness difference of the hard spot with and without hydrogen (see Figure 27) will be used to solve for how the critical crack sizes change in the hard spot with and without hydrogen. These calculations are initially being done for a 36” outside diameter by 0.312” thickness X52 pipe, typical of vintage linepipe that has experienced hard spot failures. The yield and ultimate strength of the hardspot were found in a good past NG-18 report entitled “Investigation of the Susceptibility of High-Strength Pipeline Steels to Hydrogen-Stress Cracking” NG-18 report #37, October 1972, by Tom Groeneveld et al.

We expect that these initial calculations will be completed so that the results will be in the next quarterly report. One interesting aspect of this work on hard spots is that we anticipate that as the hardness of the hard spot increases, then there is more martensite (more susceptible to hydrogen cracking per NG-18 Report #37) and the hard-spot creation stresses would be higher. That may be a double-barreled effect on failure of higher-strength hard spots. On the other hand, as the hard spot gets softer, then there is less martensite (less sensitivity to hydrogen cracking) and the hard-spot creation stresses would be lower. This should be an interesting study when completed.

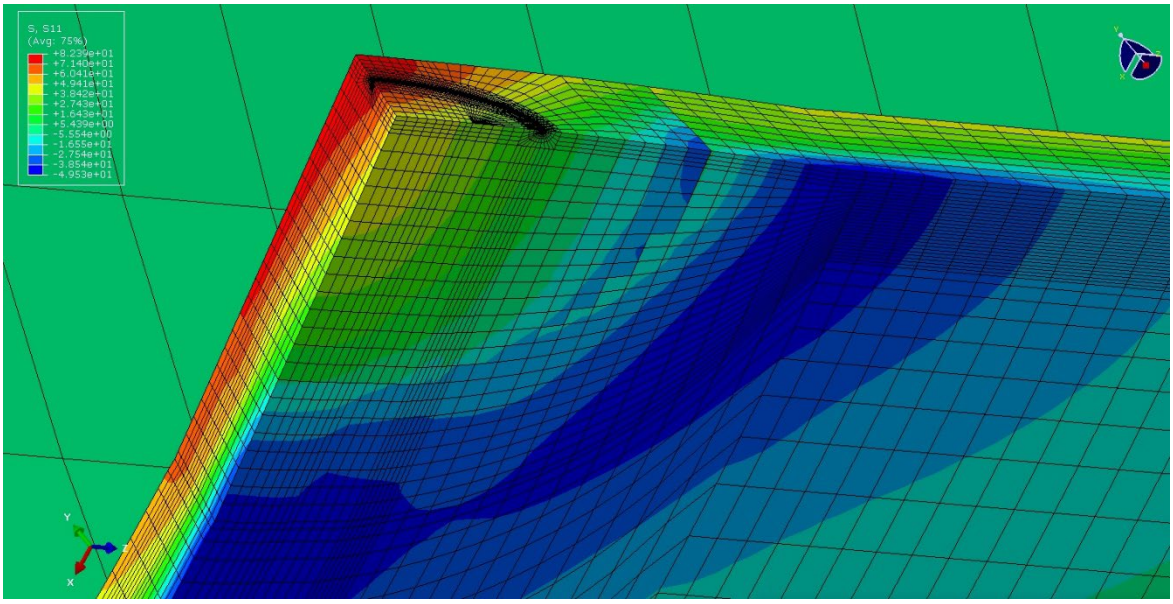

Figure 28 Initial ¼-symmetry FE mesh with OD axial surface centered in the hard spot where there is a flat in the hard spot region, 1.5% shrinkage strain in the hard spot, bending stresses from fabrication, and internal pressure

Task 6 – Review regulatory requirements for safety implications of pipeline conversion

This task is scheduled to start in the 5th quarter.

Task 7 – Determine and Describe Necessary Operator Actions

This task is scheduled to start in the 6th quarter.

5: Project Schedule

The below project GANNT chart was updated from the prior quarterly report. In the prior quarterly report, the GANNT chart was from our proposal that assumed the project started in the 3rd quarter of 2022, whereas it started in October 2022 (4th quarter of 2022).